



# Phenothiazine based co-crystals with enhanced luminescence

Luminita Marin <sup>\*</sup>, Andrei Bejan, Sergiu Shova

*"Petru Poni" Institute of Macromolecular Chemistry of Romanian Academy, Iasi, Romania*

## ARTICLE INFO

### Keywords:

Phenothiazine  
Co-crystals  
Halogen bonds  
Quantum efficiency  
Miscibility

## ABSTRACT

A series of binary phenothiazine based co-crystals were designed with the aim to reach materials with improved quantum efficiency in solid state. To this end, a host dibromine functionalized phenothiazine was mixed with a guest formyl based phenothiazine in various molar ratios, from 1:1 up to 1:9, to form single crystals and thin films as well. Single crystal X-ray diffraction, polarized light microscopy, <sup>1</sup>H NMR and FTIR spectroscopies indicated the successful formation of supramolecular synthons via halogen bonds. Polarized light microscopy and atomic force microscopy indicated the formation of submicrometric crystals into the co-crystal films. The photophysical behaviour was investigated by UV-vis and photoluminescence spectroscopies, and showed a remarkable improvement of the quantum yield, reaching values of 27% for single co-crystals and of 42% for thin films of nano-co-crystals.

## 1. Introduction

Co-crystals are hybrid materials designed in order to achieve combined properties of two or more compounds and additional/synergic properties residing from their interaction. Discovered by Wohler in 1844 [1], the organic co-crystallization emerged as an excellent strategy for better understanding of the biologic processes, e.g. protein-DNA recognition [2], lipid organization [3], protein-protein interactions which are effective in muscle contraction [4] and for improving the materials properties in view of their practical application, e.g. solubility and stability of pharmaceuticals [5–7], mechanical properties of the crystalline solids [8,9], quantum efficiency of the optical materials [10–12], charge mobility of the semiconductors [13–15], or lasing [16]. In the field of optoelectronic materials, organic co-crystallization proved to be an attractive approach for improving the luminescence and tuning the colour of emitted light. Many chromophore building blocks were used to this aim, aromatic or heteroaromatic ones, e.g. phenylene, naphthalene, anthracene, pyrene, phenantrene, fluorene, carbazole, oxadiazole, dibenzofuran, dibenzothiophene, naphthalene, phenantrolin, phenantridine, benzoquinoline [16–20]. Their combination in binary or even ternary co-crystals gave promising results which challenged the scientific community to investigate more novel mixed crystalline systems to further enrich the luminescent material family. The most spectacular results were obtained when the driving force for crystallization was the formation of halogen bonds [21,22]. It was demonstrated that the non-covalent forces between a halogen atom and

a nucleophilic site promotes the spin-orbit coupling produced by the heavy atom effect, which in turn led to an amazing increase of the quantum efficiency by activating the phosphorescence phenomenon. The effect is so effective, that outstanding results were obtained even for simple molecules based on a single aromatic ring, functionalized by bromine halogen and formyl nucleophile [10].

Phenothiazine is a fused heterocycle with strong electron-donating ability, employed in building donor-acceptor systems for electronic and opto-electronic devices, such as solar cells, field effect transistors or organic light emitting diodes [23–26]. Our group research in the synthesis and investigation of new phenothiazine derivatives revealed its promising potential for preparing materials with excellent emission in solid state, a primary necessity in building OLEDs [27–32]. Inspired by the great luminescence improvement yielded by the halogen bond driven co-crystals, we designed and prepared co-crystals based on the phenothiazine chromophore functionalized with bromine and formyl unit, respectively. The rational design was as follows.

## 2. Rational design

A series of binary co-crystals of two phenothiazine derivatives, a guest containing bromine and formyl units (7-Bromo-10-(4-hexyloxy-phenyl)-10H-phenothiazine-3-carbaldehyde (noted A)) doped into a dibromine containing host (2,7-Dibromo-10-(4-hexyloxy-phenyl)-10H-phenothiazine (noted B)), in different molar ratios, has been prepared in order to reach new materials with improved photophysical properties. In

<sup>\*</sup> Corresponding author.

E-mail address: [lmarin@icmpp.ro](mailto:lmarin@icmpp.ro) (L. Marin).

this regard, their rational design took into consideration the structural peculiarities of the two components, as follows. (i) Both compounds have the ability to grow as crystals, moreover, the A compound easily grows as single crystals and nanocrystals, from a large variety of solvents [29,31]; (ii) they are isostructural, fact which should be kinetically and thermodynamically favourable for co-crystallization, i.e. they contain a phenothiazine core and an aliphatic tail, which should facilitate their co-crystallization by rigid-flexible segregation; (iii) the two compounds have functional groups (CHO and Br) favourable for the occurrence of supramolecular synthons by halogen bonding, offering thus the predictability of co-crystals growing and good luminescence properties as well [10,22].

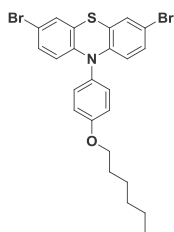
### 3. Experimental

#### 3.1. Materials

7-Bromo-10-(4-hexyloxy-phenyl)-10H-phenothiazine-3-carbaldehyde (coded A) and 2,7-Dibromo-10-(4-hexyloxy-phenyl)-10H-phenothiazine (coded B) were synthesised in our laboratory, accordingly to a published procedure [29]. Their synthesis is shortly described below. Ethyl acetate and hexane were purchased from Aldrich and dried on molecular sieves before use.

#### 3.2. Synthesis

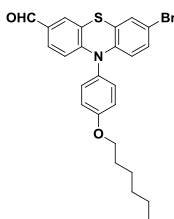
##### 3.2.1. 2,7-Dibromo-10-(4-hexyloxy-phenyl)-10H-phenothiazine (B)



In a round bottom flask were introduced sequentially: 0.5 g of 10-(4-hexyloxyphenyl)-10H-phenothiazine, 3 mL chloroform, 4.5 mL acetic acid and 0.495 g of *N*-bromosuccinimide, and then the flask was immersed in an ice bath. The reaction mixture has been vigorously stirred for 2 h, at 0 °C, under nitrogen atmosphere. After that, the organic phase was neutralized by adding 10 mL of 1% NaOH, washed three times with brine solution in a separating funnel, extracted three times with chloroform, dried on anhydrous MgSO<sub>4</sub>, filtered, and concentrated by rotary evaporation to give viscous oil. The product was purified by recrystallization from cold ethyl acetate (in a freezer) when crystals in shape of white foils, proper for diffraction, were obtained.  $\eta$  = 81%; m.p. = 106.3–108.1 °C

<sup>1</sup>H NMR (400.13 MHz, DMSO-*d*<sub>6</sub>, ppm)  $\delta$  = 7.33 (d, 2H), 7.27 (s, 2H), 7.20 (d, 2H), 7.10 (d, 2H), 6.02 (d, 2H), 4.06 (t, 2H), 1.80–1.83 (m, 2H), 1.48–1.33 (superposed bands, 6H), 0.90 (t, 3H).

##### 3.2.2. 7-Bromo-10-(4-hexyloxy-phenyl)-10H-phenothiazine-3-carbaldehyde (A)

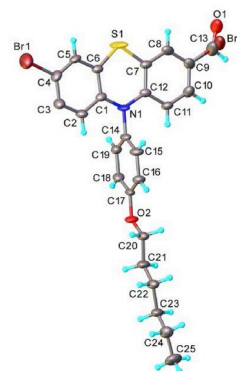


The similar procedure described above was applied for 0.3 g 10-(4-hexyloxy-phenyl)-10H-phenothiazine-3-carbaldehyde and 0.132 g *N*-

bromosuccinimide dissolved into 5.2 mL chloroform and 3.48 mL acetic acid. The product was recrystallized from ethyl acetate to give yellow greenish needle single crystals.  $\eta$  = 77%; m.p. = 147.1–150.9 °C.

<sup>1</sup>H NMR (400.13 MHz, DMSO-*d*<sub>6</sub>, ppm)  $\delta$  = 9.74 (s, 1H), 7.54 (s, 1H), 7.47 (d, 1H), 7.39 (d, 2H), 7.32 (s, 1H), 7.25 (d, 2H), 7.13 (d, 1H), 6.22 (d, 1H), 6.04 (d, 1H), 4.09 (t, 2H), 1.83–1.76 (m, 2H), 1.53–1.34 (superposed bands, 6H), 0.93 (t, 3H).

#### 3.3. Co-crystal growth



The single crystal technique provides unequivocally information related to the intermolecular forces between molecules. This is of great interest in the understanding of the structure-properties relationship which guides further studies in the design of high performance materials. This was the reason why, one of the important tasks of this work, was to grow single co-crystals suitable for X-ray analysis. To do this, we designed growing conditions considering the structure of the two components, as follows. (i) A 1/1 (v/v) mixture of polar/nonpolar solvents has been chosen as growing medium, in line with the aromatic polar part and the aliphatic nonpolar residue of A and B molecules (ii) The solution was kept in sealed vials in order to decrease the evaporation rate and thus to assure a sufficient time for co-crystal growth. This decision was done considering the weak intermolecular forces between pure A and B molecules, respectively [29], which enabled us to estimate weak intermolecular forces between them. (iii) To limit the possibility of crystallization of the pure components, and to favour the co-crystallization, the vials were kept at a relative constant temperature around 27 °C, in the darkness, in order to avoid the light radiations. After many attempts, the successful pathway towards single co-crystals was the following. A and B, in different molar ratios (Table 1), were dissolved into a 1/1 mixture of ethyl acetate/hexane to give a 1% clear solution. The solution vial was kept 1 h at 45 °C, to assure a good mixing of the two components, and then the vial was sealed and kept into a black closed box. The co-crystallization occurred at different times (Table 1), related to the content of B, i.e. longer time was necessary for higher percentage of B. The co-crystals were yellow-greenish in colour, with a more pronounced green tone as the content of B increased (Scheme 1). The single crystal X-ray diffraction confirmed the presence of the A and B components in

**Table 1**  
Single co-crystal growing conditions.

Code	A	C5	C4	C3	C2	C1	B
A/B molar ratio	100/0	50/50	40/60	30/70	20/80	10/90	0/100
A (mg)	100	50	40	30	20	10	0
B (mg)	0	50	60	70	80	90	100
EtAc/Hexane (mL)	5/5						
time (months) <sup>a</sup>	1/30 <sup>b</sup>	3	6	6	6	8	10

<sup>a</sup> Co-crystallization time.

<sup>b</sup> The crystallization occurred in 1 day.

the C1–C5 co-crystals, but only for C5 the crystal quality was enough satisfactory to reach a complete fitting of the structure and thus to provide unequivocal information. This is why, the X-ray data for C1–C4 were used for discussions, but not exhaustive presented in the paper.

**Crystal data for C5:**  $C_{24.5}H_{22.5}Br_{1.5}NO_{1.5}S$ ,  $M_r = 508.97 \text{ g mol}^{-1}$ , size  $0.30 \times 0.20 \times 0.10 \text{ mm}^3$ , triling, space group  $P-1$ ,  $a = 8.1116 (16) \text{ \AA}$ ,  $b = 8.9559 (4) \text{ \AA}$ ,  $c = 15.9838 (9) \text{ \AA}$ ,  $\alpha = 88.067 (4)^\circ$ ,  $\beta = 76.471 (5)^\circ$ ,  $\gamma = 79.330 (5)^\circ$ ,  $V = 1109.36 (11) \text{ \AA}^3$ ,  $Z = 2$ ,  $\rho_{\text{calcd}} = 1.524 \text{ g cm}^{-3}$ ,  $\mu(\text{MoK}\alpha) = 2.920 \text{ mm}^{-1}$ ,  $F(000) = 516$ , 9367 reflections in  $h(-9/9)$ ,  $k(-10/10)$ ,  $l(-19/19)$ , measured in the range  $4.628 \leq 2\theta \leq 50.05$ ,  $T = 180 \text{ K}$ , completeness  $\theta_{\text{max}} = 99.92\%$ , 39082 independent reflections,  $R_{\text{int}} = 0.0241$ , 241 parameters, 0 restraints,  $R_{1\text{obs}} = 0.0698$ ,  $wR_{2\text{obs}} = 0.0875$ ,  $R_{1\text{all}} = 0.1852$ ,  $wR_{2\text{all}} = 0.2003$ ,  $\text{GoF} = 1.041$ , largest difference peak and hole:  $0.94/-1.42 \text{ e \AA}^{-3}$ . CCDC 1965164 contain the supplementary crystallographic data for this contribution. These data can be obtained free of charge from the Cambridge Crystallographic Data Centre via [www.ccdc.cam.ac.uk/data\\_request/cif](http://www.ccdc.cam.ac.uk/data_request/cif).

In order to obtain thin films of co-crystals, the 1% clear solutions were casted on glass lamella and kept into a black closed box for two weeks, when thin depositions were obtained. The samples were noted C1f–C5f.

### 3.4. Equipment and techniques

$^1\text{H}$  NMR spectra of the **A** and **B** pure compounds and the five **C1–C5** co-crystals were registered on Bruker equipment, in  $\text{DMSO-}d_6$  solvent. In order to determine the ratio of the two components into the co-crystals, their  $^1\text{H}$  NMR spectra were recorded in triplicate, on three different single crystals, and the average molar ratio was taken as result. The ratio of the **A** guest to **B** host was calculated as  $I_{\text{B(CH}_2\text{)}}/I_{\text{A(CH}_2\text{)}}$ , where  $I_{\text{B(CH}_2\text{)}}$  represents the integral of the  $\text{CH}_2$  protons neighbour to oxygen in **B** and  $I_{\text{A(CH}_2\text{)}}$  represents the integral of the  $\text{CH}_2$  protons neighbour to oxygen in **A**. The obtained values were verified with the equation:  $(I_{\text{Ar-H}} - I_{\text{A}})/I_{\text{A}}$ , where  $I_{\text{Ar-H}}$  is the integral of the total number of the aromatic protons in co-crystal and  $I_{\text{A}}$  is the integral of the aromatic protons of **A**. For both equations,  $I_{\text{A(CH}_2\text{)}}$  and  $I_{\text{A}}$  was found setting the integral of the aldehyde proton = 1. The results were given in Table 2. They were in good agreement for both cases.

FTIR spectra were recorded on KBr pellets, using a FTIR Bruker Vertex 70 Spectrometer, at room temperature, with a resolution of  $2 \text{ cm}^{-1}$  and accumulation of 32 scans. They were processed using Opus 6.5

**Table 2**

Combination ratios of **B** and **A** in co-crystals, calculated from  $^1\text{H}$  NMR.

Code	C5	C4	C3	C2	C1
A/B ratio (expected)	1/1	1/1.5	1/2.3	1/4	1/9
A/B ratio (calculated)	1/0.97	1/1.6	1/2.3	1/4.4	1/9.4

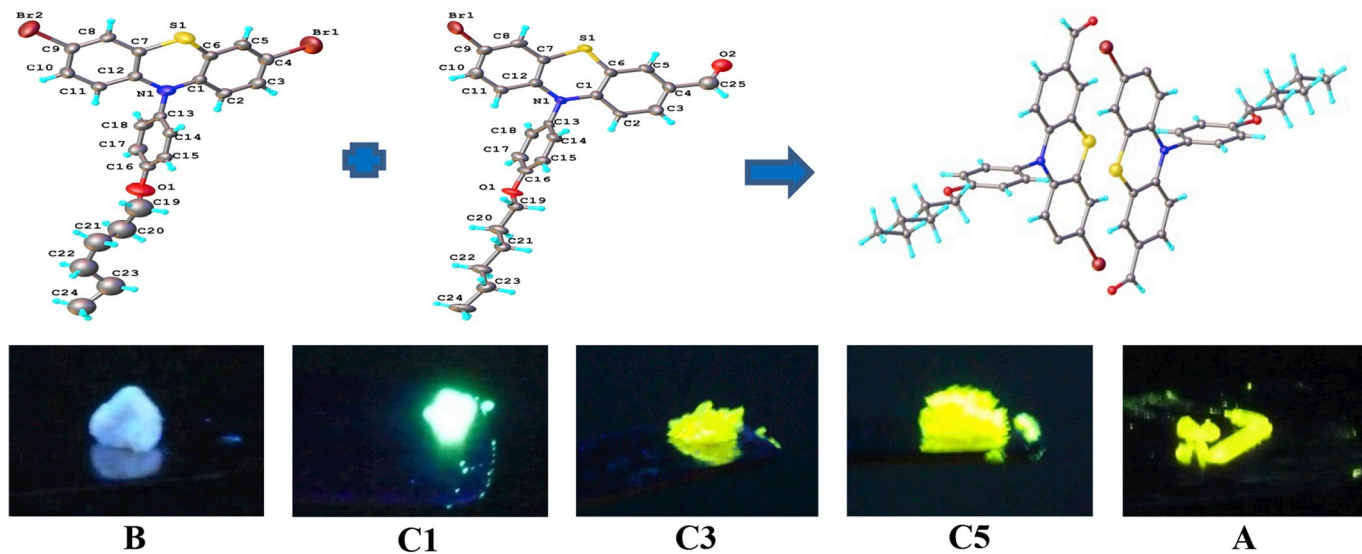
and Origin 8 software.

Crystallographic measurements for compound C5 were carried out with an Oxford-Diffraction XCALIBUR E CCD diffractometer equipped with graphite-monochromated  $\text{Mo-K}\alpha$  radiation. The single crystal was positioned at 46 mm from the detector and 506 frames were measured each for 250 s over  $1^\circ$  scan width. The unit cell determination and data integration were carried out using the CrysAlis package of Oxford Diffraction [33]. The structure was solved by direct methods using Olex2 [34] and refined by full-matrix least-squares on  $F^2$  with SHELXL-2015 [35]. Atomic displacements for non-hydrogen atoms were refined using an anisotropic model. All H atoms were introduced in idealized positions using the riding model with their isotropic displacement parameters fixed at 120% of their riding atom. The positional parameters of disordered atoms were refined in combination with PART restraints using anisotropic model for non-H atoms. When the occupancy factors for disordered bromide and aldehyde were allowed to refine they confirmed their equivalent distribution in the crystal. The molecular plots were obtained using the Olex2 program.

Atomic force microscopy images on the surface of co-crystal thin films were acquired with a Solver PRO-M, NT-MDT, Russia instrument, in semi-contact mode. Nova v.1443 software was used to record and to analyse the AFM topographic and phase contrast images.

Miscibility test, transition temperatures and textures of the co-crystals were monitored on an Axioscop 40 Zeiss polarizing optical microscope equipped with Linkam heating stage, Linksys 32 temperature control system, and QImaging/Retiga-1000R camera. For all measurements a 40x objective was used. The eyepiece has 10x magnifications. For miscibility test, equimolar amounts of **A** and **B** were deposited in contact on a glass lamella.

The absolute values of the quantum yield ( $\Phi_f$ ) were measured on a FluoroMax-4 spectrofluorometer in conjunction with a Quanta-phi integrating sphere accessory Horiba Jobin Yvon, at room temperature. The samples were excited with the light corresponding to the absorption maxima of **A** and **B** molecules in THF solution. In order to obtain a good



**Scheme 1.** Representation of the co-crystals preparation and their images under UV lamp

**Scheme 1.** Representation of the co-crystals preparation and their images under UV lamp.

optical luminescence signal-to-noise ratio, the slit width and detector parameters were optimized to maximize but not saturate the excitation Rayleigh peak.

#### 4. Results and discussions

A series of five binary co-crystals was prepared by using a mixed crystal design consisting in the combination in various molar ratios of two phenothiazine based compounds: one functionalized in 3,7 positions with bromine (**B**), and the other functionalized with bromine and formyl units (**A**) (Scheme 1). The co-crystals, abbreviated with C1–C5 codes (Table 1), were prepared as single crystals and thin films. Under an UV lamp, they emitted yellow-green light of various intensities, pointing for the encapsulation of different amounts of **A** guest in the **B** host.  $^1\text{H}$  NMR spectra of the co-crystals displayed the chemical shifting characteristic for the two components (Fig. S1), and allowed the calculation of their combination ratio (Table 2). The initial molar ratio and that calculated from NMR spectra presented a good concordance, confirming the successful encapsulation by co-crystallization of **A** guest into the **B** host. Further, FTIR spectra of the co-crystals revealed a new vibration band at  $1741\text{ cm}^{-1}$ , attributed to the occurrence of  $\text{Br}\cdots\text{O}$  halogen bonds [36]. Moreover, the vibration band of the formyl group was shifted to higher wavenumbers, from  $1676$  to  $1683\text{ cm}^{-1}$ , in accordance with the alteration of the conjugation caused by the occurrence of halogen bonding (Fig. S2).

##### 4.1. Supramolecular architecting of the co-crystals

To understand the ability of the supramolecular aggregation of co-crystals to tune their photophysical properties, the crystalline structure of the C1–C5 samples was investigated by single crystal X-ray diffraction. A previous reported structure analysis of the **A** and **B** compounds revealed specific features [29], as follows. (i) The phenothiazine core adopted an almost planar conformation (dihedral angle of  $3.4^\circ$ ) for **A** and a butterfly one, folded along the S–N vector (dihedral angle of  $23.8^\circ$ ) for **B**; (ii) The supramolecular packing of **A** and **B** molecules was governed by the  $\pi$ - $\pi$  stacking, with centroid-to-centroid distances of  $3.632$  for **A**, and  $3.820\text{ \AA}$  for **B**. (iii) The closest distance between the bromine atoms in **B** architecture was of  $5.08\text{ \AA}$ , indicating no cohesive interactions between halogens [37]. (iv) The distance between the C=O group and bromine atoms into **A** architecture was of  $3.973\text{ \AA}$ .

By comparison, in the C5 structure significant configuration alterations appeared. First, **A** and **B** molecules are crystallographic asymmetric but chemical and geometric very similar. (i) They exhibited a similar planarity of the phenothiazine core, with a dihedral angle along S–N vector of  $5.3977^\circ$ . This indicates that the intermolecular forces which governed their supramolecular packing inflicted the planarization of **B** molecules, while **A** molecules become slightly less planar. (ii) Consequently, the centroid-centroid distance was of  $3.747\text{ \AA}$ , an average value between those of pure **A** and **B** crystals. (iii) Contrary to the pure **A** and **B** crystals, the C5 co-crystal displayed quite short Br–Br contacts of  $3.646\text{ \AA}$ , indicating them as guiding forces in the packing process. (iv) Moreover, in the C1–C4 co-crystals, a main distinctive feature was the occurrence of the  $\text{Br}\cdots\text{O}=\text{CH}$ - halogen bonds, of  $2.98$  and  $2.89\text{ \AA}$  (Fig. S3), placing them among the shortest  $\text{Br}\cdots\text{O}$  halogen bonds reported in literature, indicative of electronic interactions between the two atoms, i.e. a directed heavy atom effect which may be responsible for enhancing the luminescence of co-crystals [10,38]. The occurrence of the halogen bonds appear to be responsible for the formation of supramolecular synthons which characterize the crystal packing motif. In the crystal they are further extended through  $\pi$ - $\pi$  stacking to form supramolecular ribbons, which in combination with the rigid-flexible self-assembling guided the formation of the three-dimensional supramolecular network (Fig. 1).

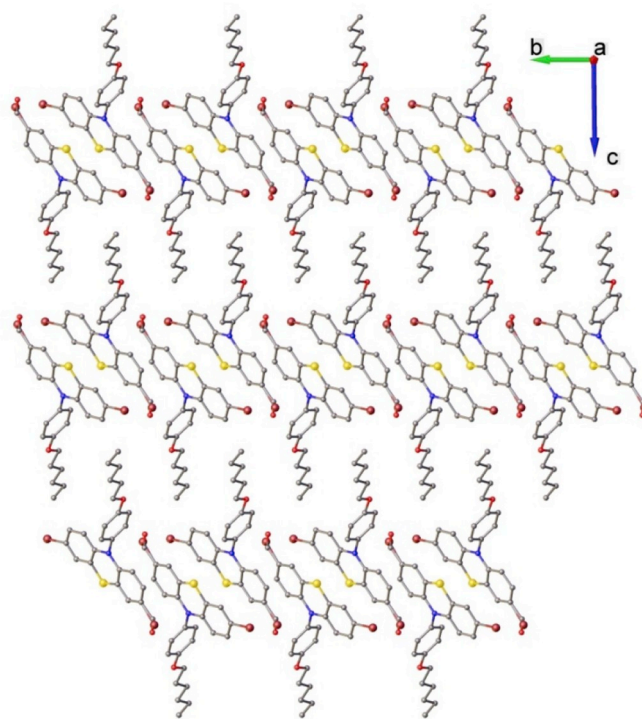
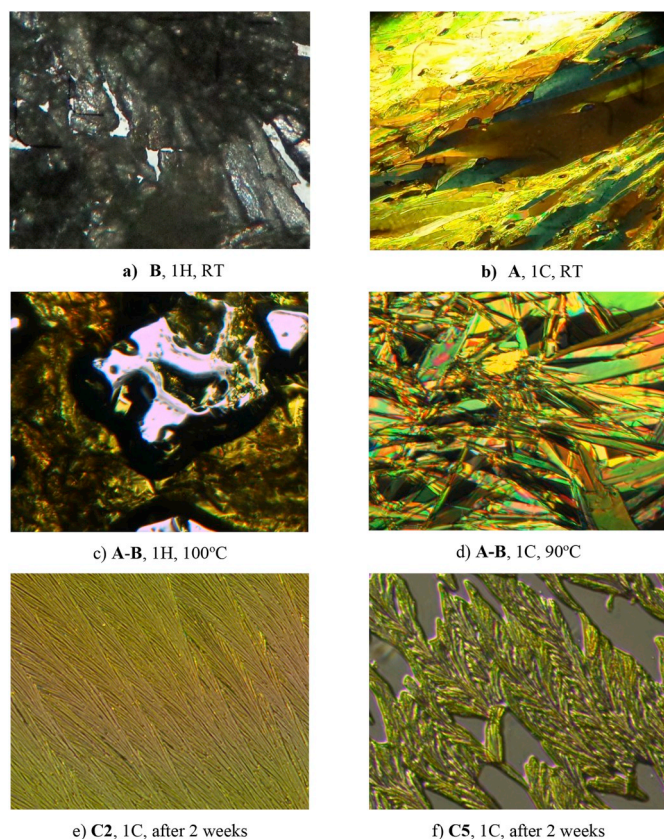


Fig. 1. View of the 3D supramolecular architecture in the C5 co-crystal structure.

##### 4.2. Morphology and thermotropic behaviour

The structural compatibility of the two compounds used for co-crystallization was investigated by a miscibility test monitored by hot stage polarized optical microscopy [39,40]. Equal amounts of **B** and **A** were placed in contact on a lamella, heated up to isotropic state and further cooled (The obtained mixed sample was noted A-B). During the heating, the **B** compound started to melt at a temperature much lower than its  $T_m$  ( $72\text{ }^\circ\text{C}$ ) and diffused towards the **A** crystals, surrounding them (Fig. 2c). The **A** crystals started to melt slowly at  $79\text{ }^\circ\text{C}$  and reached a completely isotropic phase at the temperature corresponding to the melting point of **A** ( $150\text{ }^\circ\text{C}$ ). No phase segregation was observed. Cooling down the isotropic liquid, the crystallization occurred immediately, at  $149\text{ }^\circ\text{C}$ , displaying a fast growing of board-like shapes (Fig. 2d), a crystallization pattern completely different compared to that of the pure components; **B** formed by cooling an amorphous glass, and **A** crystallized forming a continuous strong birefringent texture (Fig. 2a and b) [29]. This behaviour confirmed the structural compatibility of the two components, which led to a good miscibility, and consequently to the ability to co-crystallize together forming a new phase.

Melting point is a well-known parameter used for identification and characterization of the organic compounds, its value reflecting the intensity of intermolecular forces among the molecules. In this light, the thermotropic behaviour of the C1–C5 co-crystals has been monitored by hot stage polarized light microscopy on a heating/cooling cycle, in order to have additional information on their formation, and besides to estimate the intensity of the new forces developed between the two components. As a general remark, the co-crystals melted on a large temperature range compared to the pure components ( $10$ – $20\text{ }^\circ\text{C}$  compared to  $2$ – $3\text{ }^\circ\text{C}$ ), reflecting their discontinuous nature (Table 3). The onset of melting occurred at higher temperatures compared to that of the dibromine host, attributable to the stronger intermolecular forces developed between the two components (see *Supramolecular architecting of the co-crystals*). Moreover, the C2 melting onset was even higher than that of the **A** component, while for C2 and C3 co-crystals even the end of melting occurred at higher temperatures. During the cooling, the co-



**Fig. 2.** Optical polarized microphotographs, crossed polarizers: pure A and B precursors (a,b) and their mixture (c, d) and co-crystals (e,f) (1H: first heating; 1C: first cooling).

**Table 3**  
Thermotropic behaviour of the co-crystals and pure components.

Code	Heating		Cooling
	$T_m^{\text{onset}}$	$T_m^{\text{end}}$	
A	147	150	The crystallization process occurred at 121 °C
C1	110	120	The sample froze forming an amorphous glass.
C2	157	173	The sample froze forming an amorphous glass, which subsequently crystallized.
C3	135	155	The sample froze forming an amorphous glass, which subsequently crystallized.
C4	134	148	The sample freeze forming an amorphous glass, which subsequently crystallized.
C5	133	140	The sample freeze forming an amorphous glass, which subsequently crystallized.
B	106	108	The sample freeze forming an amorphous glass.

$T_m^{\text{onset}}$ : the melting starts at the crystals border;  $T_m^{\text{end}}$ : the sample reached a completely isotropic state.

crystals initially froze in isotropic state forming an amorphous glass, in a similar way to **B**. However, after one week **C2–C5** samples showed strong birefringent textures characteristic to the crystalline state (Fig. 2e and f). This should be correlated with the preponderance of **B** host, which hampered the occurrence of the specific intermolecular forces in viscous molten state, i.e. halogen bonds, delaying the crystallization. Nevertheless, the thermotropic behaviour confirmed the formation of the co-crystals by developing new strong intermolecular forces, i.e. halogen bonds.

Further, polarized light microscopy has been employed to investigate the phase nature of the C1f–C5f thin films. They showed a birefringent granular texture, signature of a short-range ordered phase [41]. Their heating revealed a similar behaviour to the C1–C5 co-crystals, pointing

out for a similar ordering pattern. This enables us to believe that under the pressure of the fast solvent removal, the crystallization yielded micro/nano-crystals. To have a complementary confirmation of this POM observation, the morphology of the C1f–C5f films was investigated at nano-level by atomic force microscopy. Topographic images of their surface showed a rough, granular morphology, resulted by the coalescence of sub-micrometric grains, reaching nanometric size in the case of C1 (Fig. 3, Fig. S4). Except C5f, the films showed low values of the roughness, from 15 to 24 nm, when scanning area was of  $1 \times 1 \mu\text{m}^2$ , in line with a low size of the crystals forming the films, certainly at sub-micrometric level (Table S1). Moreover the values of the roughness exponent extracted from the graphical representation of the average roughness versus scan size gave values which increased as the content of the A increased into the samples [42,43]. This suggested that the size of the crystals was correlated to the presence of A with high crystallization ability, i.e. larger crystals were obtained for higher amount of A into co-crystal. A similar trend has been showed by the average roughness measured on  $30 \times 30 \mu\text{m}^2$  (Table S1).

The data correlated well with the photophysical measurements, the best quantum yield being obtained for the **C2f** sample, which displayed the lowest roughness attributable to the smallest crystals. They should assure enough high surface-to-volume ratio, while having a reasonable amount of A to give a high percent of Br...O synthon fluorophores.

## 5. Photophysical properties

The main goal of the study was to create luminescent materials by the co-crystallization strategy, starting from phenothiazine based compounds with high quantum efficiency in solution but lacking solid-state luminescence. The effective implementation of this approach was investigated by measuring the quantum yield, in single crystal and thin film, for the C1–C5, C1f–C5f samples and their A and B precursors. The quantum yield has been measured when exciting with light of two different wavelengths, (i) 395 nm corresponding to the absorption maximum of intramolecular charge transfer (ICT) transition of A and (ii) 342 nm corresponding to the  $\pi\text{-}\pi^*$  transition of the conjugated skeleton of A, which was close to that of B (339 nm) (Fig. S5). The results were given in Table 4.

It should be noted that the high quantum yield of 66%, measured for A in solution (when excited with 342 nm) [29] was abruptly suppressed around 2% in solid state. B showed a quantum yield of 8% in solution and of 0.7% in solid state. The drastic luminescence quenching was attributed to the  $\pi\text{-}\pi^*$  stacking in solid state which favoured the non-radiative deexcitation through converting the energy to the excimer formation [29,44].

Nevertheless, the co-crystals showed a significant enhancement of the quantum yield compared to their precursor, both for single crystals and thin films (Table 4). The quantum yield reached values of 7% (C1) and 19% (C2f) when the samples were excited with light of higher energy ( $\lambda = 342 \text{ nm}$ ). A spectacular enhancement of the quantum yield values was noted when the samples were excited with the light of lower energy ( $\lambda = 395 \text{ nm}$ ), yielding values of 27% (C1) and 42% (C2f). This should be surprising considering that the ICT transition induced by exciting with light of 395 nm is less probably compared to the  $\pi\text{-}\pi^*$  transition stimulated by exciting with light of 342 nm [29]. It appears that exciting with the energy necessary for the  $\pi\text{-}\pi^*$  transition, an important loss of energy by non-radiative relaxation occurred, a phenomenon generally met for conjugated compounds in solid state [44, 45]. On the other hand, the remarkable improvement of the quantum yield when exciting with energy characteristic to the ICT transition can be correlated with the halogen bonding between the carbonyl oxygen of A molecules and bromine of A or B ones. It could be envisaged that the more localized charge of the ICT complex of A directed a better delocalization of the excited state electrons from the carbonyl oxygen to the outer orbitals of the heavy bromine atoms facilitating the spin-orbit coupling, and therefore amplifying the radiative deactivation by

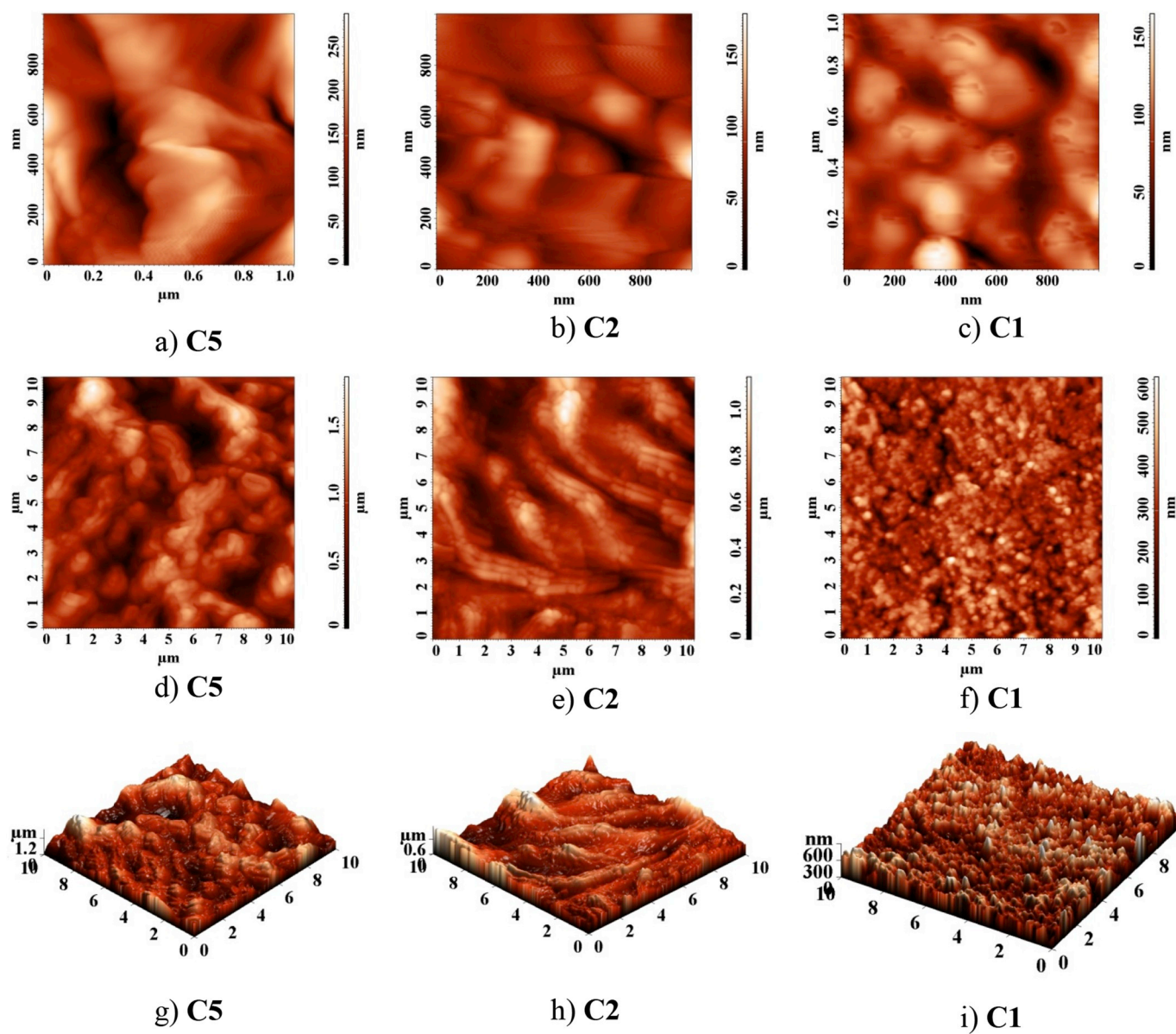


**Figure 3.** Representative AFM images of the co-crystal films

Fig. 3. Representative AFM images of the co-crystal films.

**Table 4**  
Quantum yield (QY) values of the studied samples.

Code	QY <sub>sc</sub>		Code	QY <sub>film</sub>		Code	QY <sub>physical mixture</sub>	
	$\lambda_{ex}$ : 395	$\lambda_{ex}$ : 342		$\lambda_{ex}$ : 395	$\lambda_{ex}$ : 342		$\lambda_{ex}$ : 395	$\lambda_{ex}$ : 342
A	4.2	2.12	Af	2.33	1.72	A	–	–
C5	11.2	3.7	C5f	3.3	3.7	A-B (1:1)	1.2	0.39
C4	13.6	5.3	C4f	12.9	8.2	A-B (1:1.5)	2.53	1.54
C3	17.2	6.07	C3f	33.4	14.2	A-B (1:2.3)	2.35	0.72
C2	17.3	8.8	C2f	42	19.9	A-B (1:4)	4.04	0.68
C1	27.1	7.8	C1f	37.8	12.02	A-B (1:9)	4.74	0.71
B	–	0.7	Bf	–	2.18	B	–	–

QY<sub>sc</sub>: quantum yield determined on the C1–C5 single crystal samples; QY<sub>film</sub>: quantum yield determined on the C1f–C5f film samples. QY<sub>p</sub>: quantum yield determined on the physical mixture of the A and B components grinded together, in the corresponding molar ratio given in brackets; For both samples, the QY was measured when excited with light of 395 nm - characteristic to the intramolecular charge transfer transition in A, and 342 nm - characteristic to the  $\pi$ - $\pi^*$  transition of the conjugated system of A and B.

phosphorescence. Complementary, the non-radiative deactivation channels could be limited, due to the lower transition energy compared to that of the conjugated skeleton. Considering the supramolecular

structure of the co-crystals, it should be regarded that the positive effect of the halogen bonding on the quantum efficiency overcame the self-quenching favoured by the  $\pi$ - $\pi^*$  stacking.

To highlight the importance of co-crystallization on the luminescence efficiency, the quantum yield has been measured on powder of the two components grinded together in the corresponding molar ratio (Table 4). The quantum yield presented values even lower than those of the pure crystals, supporting the hypothesis of the positive influence of halogen bonding on the quantum efficiency.

Contrary to other reported data, the C1f–C5f thin films showed higher quantum yield than the single co-crystals [10]. This was attributed to the larger surface-to volume ratio raised by the multitude of small co-crystals compared to that of a unique co-crystal. The better quality of the co-crystals favoured by the great crystallization potential of the phenothiazine based derivatives should play also an important role to this.

Comparing the values of the quantum yield, it can be remarked an increasing trend, as the amount of A guest into B host decreased. This was associated with the formation of smaller co-crystals into the crystal of B host [11], inducing a solid solution -like effect [31,46,47].

Looking to the emission spectra, significant differences of the emission maximum were observed between the C1–C5 single co-crystals and C1f–C5f co-crystal films compared to those of the pure components (Fig. 4). Thus, while the A crystal has an emission maximum at 550 nm and B crystal at 480 nm, the emission maximum of the C1–C5 single co-crystals and C1f–C5f thin films lays at intermediate values, around 507 and 518 nm, respectively. This indicates a new fluorophore responsible for emission, i.e. the new formed supramolecular synthons. The shifting

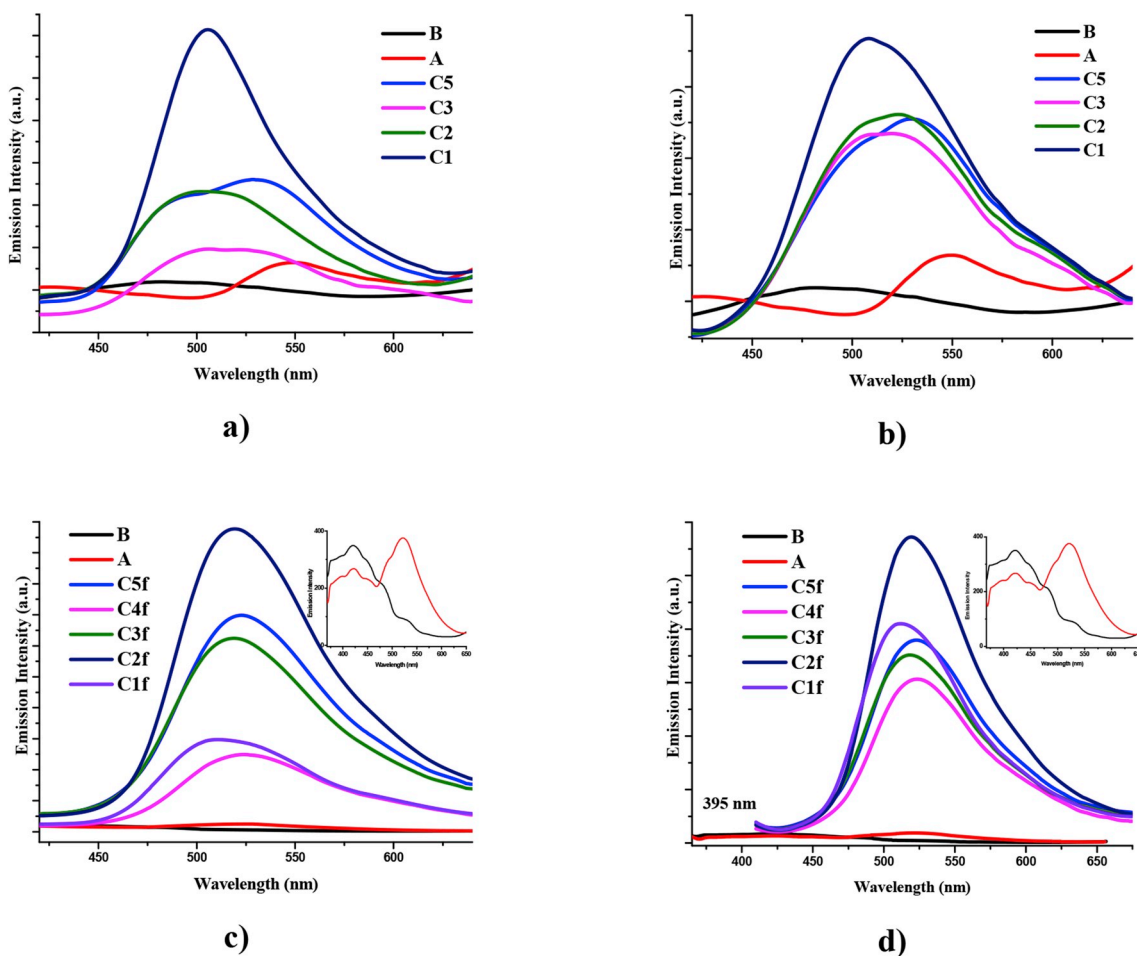


**Fig. 4.** Emission spectra of the single C1–C5 co-crystals when excited at (a) 342 nm and (b) 395 nm and of the C1f–C5f co-crystal films when excited at (c) 342 nm and (d) 395 nm.

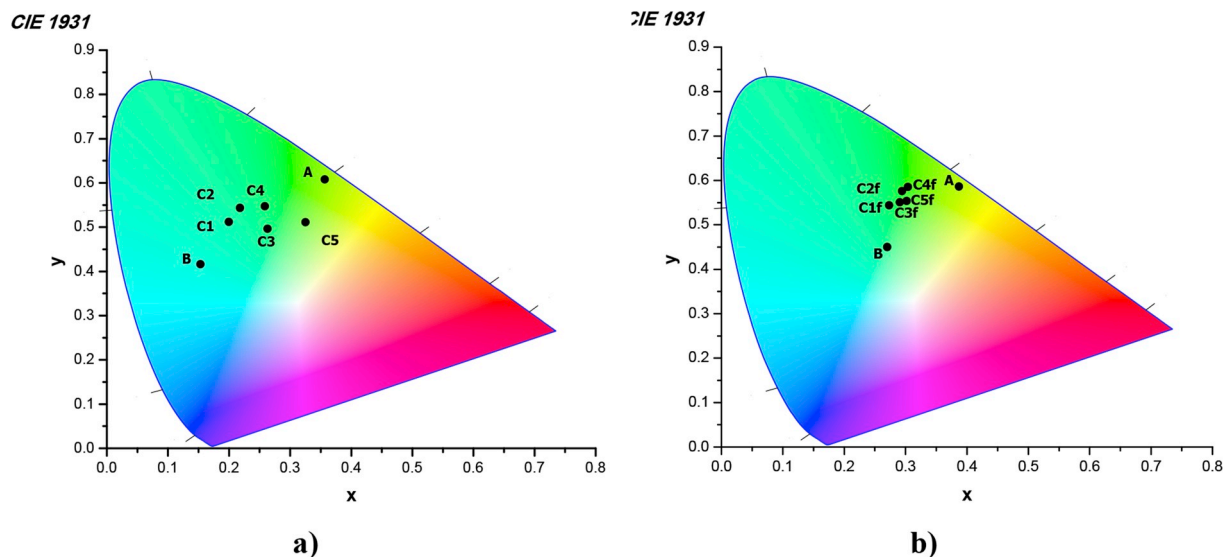


Fig. 5. Chromaticity diagram of the studied samples when excited with 420 nm as (a) co-crystals and (b) co-crystal films.

of the emission maximum was correspondingly accompanied by the change of the colour of the emitted light. In the chromaticity diagrams, the colour of light emitted by C1–C5 co-crystals positioned in the green visible region, spanning between the yellowish-green of A crystals and the bluish-green of B crystals (Fig. 5a). In the film state, the C1f–C5f emission colour shifted more to the green-yellow domain, phenomenon encountered for nano-crystalline materials, which show a close correlation between size and colour of emitted light [31,48,49].

## 6. Conclusions

The study demonstrated the co-crystallization guided by halogen bonding as an excellent strategy for improving the quantum efficiency in solid state of the isostructural phenothiazine derivatives. This main conclusion was drawn from the correlation of the structural, supramolecular, thermotropic and photophysical data obtained for a series of binary co-crystals prepared from bromine and formyl functionalized phenothiazine derivatives in various molar ratios. It was demonstrated that combination of the phenothiazine donor with a formyl acceptor promotes the charge delocalization, which is beneficial for halogen bonding and thus luminescence improving. The study is an important step towards solid state materials with high luminescence efficiency for organic light emitting diodes.

## Declaration of competing interest

The authors declare that they have no known competing financial interests or personal relationships that could have appeared to influence the work reported in this paper.

## CRediT authorship contribution statement

**Luminita Marin:** Conceptualization, Data curation, Funding acquisition, Methodology, Project administration, Supervision, Writing - original draft, Writing - review & editing. **Andrei Bejan:** Formal analysis, Investigation, Software. **Sergiu Shova:** Formal analysis, Investigation, Software, Writing - original draft.

## Acknowledgments

The paper is part of a project financed through a Romanian National Authority for Scientific Research MEN – UEFISCDI grant, project number PN-III-P1-1.2-PCCDI2017-0917, 21PCCDI/2018 and through the

European Union's Horizon 2020 research and innovation programme under grant agreement 667387.

## Appendix A. Supplementary data

Supplementary data to this article can be found online at <https://doi.org/10.1016/j.dyepig.2019.108164>.

## References

- [1] Wohler F. Untersuchungen über das Chinon. *Justus Liebigs Ann Chem* 1844;51(2): 145–63.
- [2] Jordan SR, Whitcombe TV, Berg JM, Pabo CO. Systematic variation in DNA length yields highly ordered repressor-operator cocrystals. *Science* 1985;230:1383–5.
- [3] Short KW, Wallace BA, Myers RA, Fodor SPA, Dunker AK. Comparison of lipid/gramicidin dispersions and cocrystals by Raman-scattering. *Biochemistry* 1987;26: 557–62.
- [4] Carr HJ, O'Brien EJ, Morris EP. Structure of tropomyosin-troponin T cocrystals. *J Muscle Res Cell Motil* 1988;9:384–92.
- [5] Williams HD, Trevaskis NL, Charman SA, Shanker RM, Charman WN, Pouton CW, Porter CJH. Strategies to address low drug solubility in discovery and development. *Pharmacol Rev* 2013;65:315–499.
- [6] Trask AV, Motherwell WDS, Jones W. Physical stability enhancement of theophylline via cocrystallization. *Int J Pharm* 2006;320:114–23.
- [7] Schultheiss N, Newman A. Pharmaceutical cocrystals and their physicochemical properties. *Cryst Growth Des* 2009;9:2950–67.
- [8] Mukherjee A, Tothadi S, Desiraju GR. Halogen bonds in crystal engineering: like hydrogen bonds yet different. *Acc Chem Res* 2014;47:2514–24.
- [9] Karki S, Friscic T, Fabian L, Laity PR, Day GM, Jones W. Improving mechanical properties of crystalline solids by cocrystal formation: new compressible forms of Paracetamol. *Adv Mater* 2009;21:3905–9.
- [10] Bolton O, Lee K, Kim HJ, Lin KY, Kim J. Activating efficient phosphorescence from purely organic materials by crystal design. *Nat Chem* 2011;3:205–10.
- [11] Bolton O, Lee D, Jung J, Kim J. Tuning the photophysical properties of metal-free room temperature organic phosphors via compositional variations in bromobenzaldehyde/dibromobenzene mixed crystals. *Chem Mater* 2014;26: 6644–9.
- [12] Usman R, Khan A, Wang ML, Luo Y, Sun WW, Sun H, et al. Investigation of charge-transfer interaction in mixed stack donor-acceptor cocrystals toward tunable solid-state emission characteristics. *Cryst Growth Des* 2018;18:6001–8.
- [13] Ferraris J, Cowan DO, Walatka Jr V, Perlstein JH. Electron transfer in a new highly conducting donor-acceptor complex. *J Am Chem Soc* 1973;95:948–9.
- [14] Arkalekha M, Anwasha C, Parameswar KI, Prasenjit M. Charge transfer versus arene-perfluoroarene interactions in modulation of optical and conductivity properties in cocrystals of 2,7-di-tert-butylpyrene. *J Phys Chem C* 2019;123: 18198–206.
- [15] Huang YJ, Wang ZR, Chen Z, Zhang QC. Organic cocrystals: beyond electrical conductivities and field-effect transistors (FETs). *Angew Chem Int Ed* 2019;58: 9696–711.
- [16] Yu Y, Li Z-Z, Wu J-J, Wei G-Q, Tao Y-C, Pan M-L, et al. Transformation from nonlasing to lasing in organic solid-state through the cocrystal engineering. *ACS Photonics* 2019;6:1798–803.

- [17] Sun H, Peng J, Zhao K, Usman R, Khan A, Wang M. Efficient luminescent microtubes of charge-transfer organic cocrystals involving TCNB, carbazole derivatives and pyrene derivatives. *Cryst Growth Des* 2017;17:6684–91.
- [18] Khan A, Usman R, Sayed SM, Li R, Chen H, He N. Supramolecular design of highly efficient two-component molecular hybrids toward structure and emission properties tailoring. *Cryst Growth Des* 2019;19:2772–8.
- [19] Liu JJ, Liu T, Xia SB, He CX, Cheng FX, Lin MJ, et al. Luminescence cocrystals of naphthalene diimide with naphthalene derivatives: a facile approach to tune the luminescent properties. *Dyes Pigments* 2018;149:59–64.
- [20] Zhang HC, Guo EQ, Zhang YL, Ren PH, Yang WJ. Donor–Acceptor-Substituted anthracene-centered cruciforms: synthesis, enhanced two-photon absorptions, and spatially separated frontier molecular orbitals. *Chem Mater* 2009;21:5125–35.
- [21] Goswami A, Garai M, Biradha K. Interplay of halogen bonding and hydrogen bonding in the cocrystals and salts of dihalogens and trihalides with N,N'-bis(3-pyridylacrylamido) derivatives: phosphorescent organic salts. *Cryst Growth Des* 2019;19:2175–88.
- [22] Priimagi A, Cavallo G, Metrangolo P, Resnati G. The halogen bond in the design of functional supramolecular materials: recent advances. *Acc Chem Res* 2013;46(11):2686–95.
- [23] Huang ZS, Meier H, Cao D. Phenothiazine-based dyes for efficient dye-sensitized solar cells. *J Mater Chem C* 2016;4:2404–26.
- [24] Okazaki M, Takeda Y, Data P, Pander P, Higginbotham H, Monkman AP, et al. Thermally activated delayed fluorescent phenothiazine-dibenzo[a,j]phenazine-phenothiazine triads exhibiting tricolor-changing mechanochromic luminescence. *Chem Sci* 2017;8:2677–86.
- [25] Hwang DH, Kim SK, Park MJ, Lee JH, Koo BW, Kang IN, et al. Conjugated polymers based on phenothiazine and fluorene in light-emitting diodes and field effect transistors. *Chem Mater* 2004;16:1298–303.
- [26] Shi J, Xu L, Chen C, Lv X, Ding Q, Li W, et al. Efficient and color-purity blue electroluminescence by manipulating the coupling forms of D–A hybrids with phenothiazine as the strong donor. *Dyes Pigments* 2019;160:962–70.
- [27] Zabolica A, Balan M, Bele D, Sava M, Simionescu BC, Marin L. Novel luminescent phenothiazine-based Schiff bases with tuned morphology. Synthesis, structure, photophysical and thermotropic characterization. *Dyes Pigments* 2013;96:686–92.
- [28] Bele D, Dumea C, Bicu E, Marin L. Phenothiazine and pyridine-N-oxide-based AIE-active triazoles: synthesis, morphology and photophysical properties. *RSC Adv* 2015;5:8849–58.
- [29] Bejan A, Shova S, Damaceanu MD, Simionescu BC, Marin L. Structure-directed functional properties of phenothiazine brominated dyes: morphology and photophysical and electrochemical properties. *Cryst Growth Des* 2016;16:3716–30.
- [30] Marin L, Bejan A, Ailincăi D, Bele D. Poly(azomethine-phenothiazine)s with efficient emission in solid state. *Eur Polym J* 2017;95:127–37.
- [31] Bejan A, Marin L. Phenothiazine based nanocrystals with enhanced solid state emission. *J Mol Liq* 2018;265:299–306.
- [32] Bejan A, Ailincăi D, Simionescu BC, Marin L. Chitosan hydrogelation with a phenothiazine based aldehyde: a synthetic approach toward highly luminescent biomaterials. *Polym Chem* 2018;9:2359–69.
- [33] CrysAlis RED. Oxford Diffraction Ltd; 2003. Version 1.171.36.32.
- [34] Dolomanov OV, Bourhis LJ, Gildea RJ, Howard JAK, Puschmann H. OLEX2: a complete structure solution, refinement and analysis program. *J Appl Crystallogr* 2009;42:339–41.
- [35] Sheldrick GM. Crystal structure refinement with SHELXL. *Acta Crystallogr C* 2015;71:3–8.
- [36] Yan D, Delori A, Lloyd GO, Friščić T, Day GM, Jones W, et al. A cocrystal strategy to tune the luminescent properties of stilbene-type organic solid-state materials. *Angew Chem Int Ed* 2011;50:12483–6.
- [37] Marin L, Harabagiu V, van der Lee A, Arvinte A, Barboiu M. Structure-directed functional properties of symmetrical and unsymmetrical Br-substituted Schiff-bases. *J Mol Struct* 2013;1049:377–85.
- [38] Metrangolo P, Resnati G. Halogen bonding: a paradigm in supramolecular chemistry. *Chem Eur J* 2001;7:2511–9.
- [39] Mitsuo F, Kenichi T, Kato T. Preliminary communication - miscibility of a hydrogen-bonded mesogenic complex with normal liquid crystals. *Liq Cryst* 1998;24:325–7.
- [40] Zabolica A, Perju E, Bruma M, Marin L. Novel luminescent liquid crystalline polyazomethines. Synthesis and study of thermotropic and photoluminescent properties. *Liq Cryst* 2014;41:252–62.
- [41] Marin L, Zabolica A, Sava M. New symmetric azomethinic dimer: the influence of structural heterogeneity on the liquid crystalline behaviour. *Liq Cryst* 2011;38:433–40.
- [42] Macanas J, Palacio L, Pradanos P, Hernandez A, Munoz M. Atomic force microscopy as a suitable technique for surface characterization of activated composite membranes for metal ion facilitated transport. *Appl Phys A* 2006;84:277–84.
- [43] Marin L, Timpu D, Cozan V, Rusu GI, Airinei A. Solid state properties of thin films of new copoly(azomethine-sulfone)s. *J Appl Polym Sci* 2011;120:1720–8.
- [44] Chen Y, Lam JWY, Kwok RTK, Liu B, Tang BZ. Aggregation-induced emission: fundamental understanding and future developments. *Mater Horiz* 2019;6:428–33.
- [45] Albagli D, Bazan GC, Schrock RR, Wrighton MS. New functional polymers prepared by ring-opening metathesis polymerization: study of the quenching of luminescence of pyrene end groups by ferrocene or phenothiazine centers in the polymers. *J Phys Chem* 1993;97:10211–6.
- [46] Malina I, Kampars V, Belyakov S. Luminescence properties of 2-benzoyl-1,3-indandione based Eu<sup>3+</sup> ternary and tetrakis complexes and their polymer films. *Dyes Pigments* 2018;159:655–65.
- [47] Sun Q, Zhang K, Zhang Z, Tang L, Xie Z, Chi Z, et al. A simple and versatile strategy for realizing bright multicolor mechanoluminescence. *Chem Commun* 2018;54:8206–9.
- [48] Zrazhevskiy P, Sena M, Gao X. Designing multifunctional quantum dots for bioimaging, detection, and drug delivery. *Chem Soc Rev* 2010;39:4326–54.
- [49] Marin L, Zabolica A, Moleavin I-A. Luminescent guest-host composite films based on an azomethine dye in different matrix polymers. *Opt Mater* 2014;38:290–6.